ACS Biomaterials SCIENCE & ENGINEERING

pubs.acs.org/journal/abseba

Article

Enhancing Paracellular Permeability of Airway Epithelium by Opening Tight Junctions via Osmo-Mechanical Stimulation

Aneri Patel, Jiawen Chen, Mohammad Mir, Maria R. Hudock, Meghan R. Pinezich, Ya-Wen Chen, Matthew Bacchetta, Gordana Vunjak-Novakovic, and Jinho Kim*

Cite This: https://doi.org/10.1021/acsbiomaterials.5c01104

Read Online

ACCESS | Metrics & More | Article Recommendations | Supporting Information

ABSTRACT: Pulmonary drug delivery offers significant advantages for local and systemic therapy by directly targeting the lungs, minimizing off-target effects and avoiding first-pass metabolism. However, the airway epithelium, which serves as a protective barrier, presents significant challenges for effective drug delivery. Tight junctions (TJs) between epithelial cells and mucociliary clearance hinder drug absorption, especially for high-molecular-weight drugs. To address this, various TJ modulators, such as chelators and surfactants, have been explored but their safety concerns limit clinical application. In clinical settings, hyperosmotic sodium chloride (NaCl) and mechanical vibration are used for mucus clearance, but their effects on the TJ permeability remain underexplored. In this study, we investigate the synergistic effects of hypertonic saline (HTS) solution (1.8% NaCl) and mechanical vibration (frequency: 70 Hz; duration: 30 min) on the opening of TJs in the rat tracheal epithelium. Our results show that this combination effectively increases the epithelial permeability, offering a novel and safe strategy for enhancing pulmonary drug delivery. This work provides insights into utilizing established clinical techniques to overcome barriers in pulmonary drug administration, paving the way for more effective treatments.

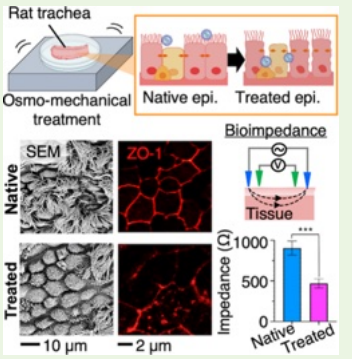

KEYWORDS: *respiratory drug delivery, lung disease, airway tissue permeability, tight junction opening*

Downloaded via Jinho Kim on October 5, 2025 at 17:39:27 (UTC).
See https://pubs.acs.org/sharingguidelines for options on how to legitimately share published articles.

1. INTRODUCTION

Drug delivery across pulmonary epithelia is a promising route for local and systemic therapy.[1,2] Pulmonary drug delivery allows for the direct delivery of high concentrations of drugs to the site of action, reducing potential off-target effects in other organs, avoiding first-pass metabolism, and eventually resulting in a rapid response with the reduced risk of systemic side effects.[3−8] Unlike systemic administration, the pulmonary route offers the advantages of being minimally invasive and suitable for delivery of a wide range of molecules, such as proteins and nucleic acids, due to the absence of digestive enzymes found in oral administration.[9−12] However, the airway epithelium lining of the respiratory tract serves as a protective barrier for lungs, creating challenges for effective pulmonary administration. For example, the mucociliary flow, crucial barrier functions of the airway epithelium, can trap and expel drugs from the respiratory tract.[13−15] Additionally, tight junctions (TJs) formed between epithelial cells (Figure 1A) form the defensive barrier, further limiting drug absorption.[16,17] To achieve effective pulmonary drug delivery, new safe approaches are needed to overcome these challenges.

To overcome TJ barrier and increase drug absorption, TJ modulators, such as chelators, surfactants, fatty acids and TJ toxins, have been used to modulate TJ permeability.[18−22] For example, McCray's group has shown that the combination of calcium chelator ethyleneglycol-bis(2-aminoethyl ether)-*N*,*N*,*N*′,*N*′-tetra acetic acid (EGTA) and hypotonic buffer

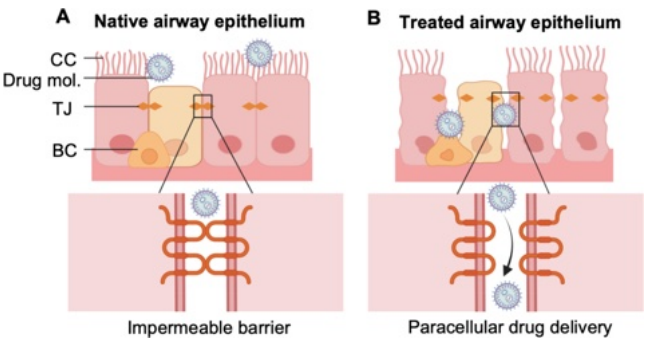

Figure 1. Schematics of the TJ structure and NaCl with a mechanical stress working mechanism. (A) Healthy epithelial layer of an airway with intact TJ making it difficult for paracellular drug delivery. (B) After treatment of hyperosmotic pressure and vibrational force, the TJ are disrupted, promoting paracellular drug delivery. CC: ciliated cells, TJ: tight junction, BC: basal cells, and mol.: molecules.

Received: June 18, 2025
Revised: September 24, 2025
Accepted: September 25, 2025

© XXXX The Authors. Published by American Chemical Society

could modulate the permeability of airway epithelial TJ and enhanced gene transfer.[18] While these modulators have demonstrated promise in overcoming the challenges posed by TJs for drug delivery, their applications also raise significant safety concerns. Prolonged exposure or high doses of TJ modulators may cause irreversible damage to TJs, hindering their clinical translation.[21]

In clinics, hyperosmotic sodium chloride (NaCl) and mechanical vibration are used to remove mucus from airways.[23] Additionally, hypertonic solutions can open TJs between airway epithelial cells.[19,20,24,25] The mechanism behind this effect may involve cell shrinkage induced by osmotic stress, which alters organization of TJ proteins, leading to TJ disruption.[20,24] Simultaneously, vibration treatment can destabilize the TJ proteins, leading to an increased paracellular permeability. This is because the vibration can induce mechanical stress on cells, causing alterations in cellular actin cytoskeleton that interacts with TJ proteins to maintain their structure and function, leading to the modulation of TJs[26,27] (Figure 1B).

Although the combination of hyperosmotic NaCl and mechanical vibration has been deployed for clearing mucus in clinics, the influence of this approach on permeability of TJs remains to be investigated. Thus, in this study, we explored the synergistic effects of hypertonic saline (HTS) solution (1.8% NaCl) and mechanical vibration (frequency: 70 Hz) on modulation of TJs for enhancement of permeability of the airway epithelium. We assessed one of TJ proteins (zonula occludens-1), cilia, electrical impedance, and paracellular permeability of the rat tracheal epithelium after our osmo-mechanical treatment. Excitingly, the results demonstrate that this combination can effectively modulate TJs and increase the permeability of epithelial cells. To the best of our knowledge, this is the first time that this clinical airway clearance therapy has been applied to increase epithelial junction permeability. Meanwhile, our work also offers a safe and feasible strategy for overcoming the challenges associated with pulmonary drug delivery.

2. METHODS

2.1. Isolation of the Rat Trachea. This study utilized Sprague−Dawley rats (SAS SD Rats, Charles River Laboratories, weight: 200−250 g). All animal procedures were conducted in accordance with an animal protocol approved by the Institute for Animal Care and Use Committee (IACUC) (Protocol number: 2023-002 (AP)) at Stevens Institute of Technology. Freshly isolated rat tracheae were used for the experiments. Rats were euthanized with a 5% isoflurane overdose for 20 min, followed by the removal of connective tissues and gentle washing of the tracheae with 1× phosphate-buffered saline (PBS) (cat. no. 10-0044, Sakura Genemed) to remove blood. The washed tracheae were then stored in PBS until they were used for the subsequent experiments using 1.8% sodium chloride (NaCl) (cat. no. 7647-14-15, ThermoFisher scientific) and 70 Hz Vibrational force for 30 min.

2.2. Custom-Designed Electromagnetic Shaker. The experimental setup utilized an electromagnetic shaker built on a translational stage (TBB1212, ThorLabs). The actuator (TT25-8 PUCK, Dayton audio) was secured between two acrylic plastic sheets, which were supported by holders and posts. An accelerometer (WT61C, WitMotion) was positioned on top of the stage to measure vibrations. The actuator of the shaker was connected to an amplifier (K3118, Kinter), which in turn was linked to a computer for control and data acquisition.

2.3. HTS with Vibration Treatment. After the rat tracheal tissue was isolated, it was placed in a Petri dish and exposed to 1.8% hypertonic NaCl diluted in DI water. The dish was then placed on an electromagnetic shaker for 30 min periods and exposed to a computer-generated sinusoidal wave with a frequency of 70 Hz. The frequency and amplitude of the actuator were adjusted by using the computer and amplifier. An accelerometer was employed to continuously monitor the response of the actuator, ensuring an accurate delivery of the vibrational force.

2.4. Immunofluorescent Staining. Rat tracheae were isolated, sectioned, and subjected to experimental treatments. Tissue sections were fixed in 4% paraformaldehyde (cat. no. 30525-89-4, Thermofisher Scientific) overnight to preserve the tissue architecture. Nonspecific binding sites were blocked with 0.5% BSA (cat. no. 9048-46-8, VWR) and 0.5% Triton X-100 (cat. no. 9002-93-01, VWR) in PBS for 1 h at room temperature. Antibodies for ZO-1 (cat. no. sc-33725, Santa Cruz Biotechnology) and for cilia (cat. no. SAB5600134, Sigma-Aldrich) were then applied to the sections and incubated overnight at 4 °C, following three washes with 0.5% Triton X-100 in PBS. After additional washes, nuclear staining was performed using DAPI (4′,6-diamidino-2-phenylindole) (cat. no. ab228549, Abcam) for 15 min, followed by final washes. Slides were mounted with an antifade mounting medium (cat. no. H-1700-10, Vector Laboratories) for subsequent confocal microscopy analysis using an LSM 880, Zeiss. This protocol enabled the visualization and localization of target proteins within tracheal tissue.

2.5. Quantification of ZO-1 and Cilia. Initially, the image was converted to grayscale and subjected to appropriate thresholding (for this experiment, min value: 39 intensity, max value: 255 intensity) to differentiate the stained region from the background. Subsequently, a parameter counting tool was employed to measure the total area of the stained region. The area fraction index for the threshold image was calculated by dividing the area of positive staining by the total area of the image, providing a quantitative assessment of protein expression and distribution within the tissue. This analysis was performed on multiple images per experimental condition to ensure statistical reliability.

2.6. Scanning Electron Microscopy (SEM) of Airway Lumen. The luminal surface of the tracheal tissue was treated and visualized via a scanning electron microscope (SEM). The tissues were cut into small tissue samples and fixed using 2.5% glutaraldehyde (cat. no. 16520, Electron Microscopy Science) at pH 7.0 overnight at 4 °C. The fixed tissue were then washed three times for 5 min each with 1X PBS and dehydrated with a graded series of aqueous ethanol solution concentrations: 25, 50, 70, 85, 95, and 100% (v/v). The tissues were kept in a hexamethyldisilane solvent overnight in a fume hood. The tissues were airdried and then coated with gold using a sputter coater. The samples were now ready to be imaged using scanning electron microscopy (SEM) with an accelerated voltage of 2 kV.

2.7. Epithelial Barrier Function Test. The permeability assay was performed on native and treated tissues. We used 2 mg/mL fluorescein isothiocyanate−dextran (3−5 kDa, cat. no. 60842-46-8, Sigma-Aldrich). After the treatment, the tissue were exposed to diluted dextran molecules in DI water for 15 min and was washed with 1X PBS. The samples were then fluorescently labeled with DAPI and ZO-1 antibody to localize the penetration depth of the dextran in the epithelial layer of airway tissue. The stained samples were visualized in the confocal microscopy.

2.8. Bioimpedance Measurement System. Electrical properties of the rat trachea were assessed by using a precision LCR meter (E4980AL, Keysight). To enhance the measurement accuracy, we implemented a four-probe technique. During measurements, electrodes make direct contact with the tissue to assess its electrical characteristics. An alternating electrical current (AC) with varying frequencies (250 Hz to 135 kHz) and a maximum amplitude of 100 μA was supplied into the tissue using two current-carrying electrodes. Two voltage pick-up electrodes simultaneously measured the potential distribution at the measurement site. We quantified the obtained electrical resistance (R) and reactance (X) across the entire frequency range, but our analysis focused on data collected at 120 kHz. The acquired data were then used to calculate bioimpedance (Z) using the:

https://doi.org/10.1021/acsbiomaterials.5c01104
ACS Biomater. Sci. Eng. XXXX, XXX, XXX−XXX

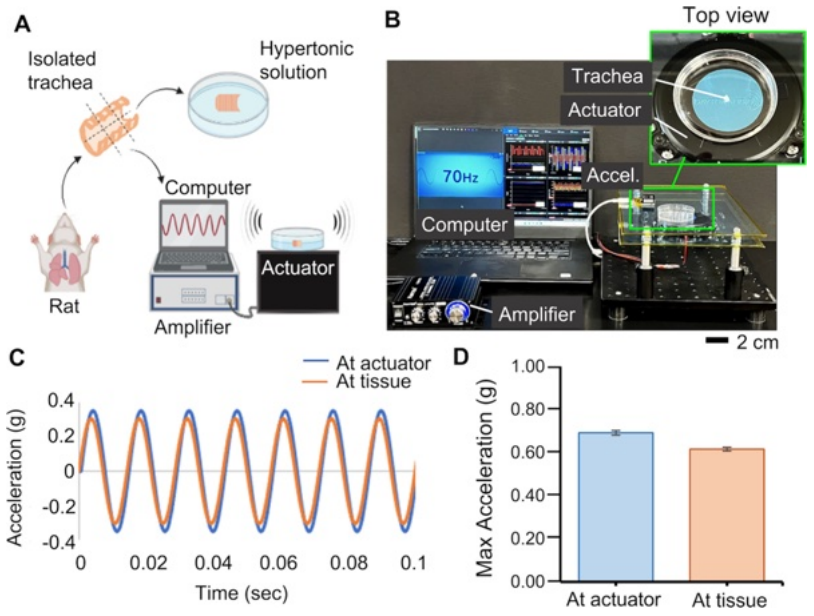

Figure 2. Experimental setup for disrupting TJ. (A) Schematics of the method with combined treatment of hyperosmotic pressure and mechanical stress. (B) Photograph of the experimental setup. (C) Quantifying input and output acceleration vs time for the vibrational force. (D) Bar graph showing the input and output accelerations of the vibrational force.

$$Z = R + jX, \text{ where } |Z| = \sqrt{R^2 + X^2}$$

Four tungsten electrodes (SE-T, Lucas Signatone; length: 30 mm; tip diameter: 5 μm) were strategically positioned using micro positioners (S-725SLM or S-725SRM, Lucas Signatone), ensuring precise placement. The electrode tip positions were monitored in real-time using a custom-built microscope equipped with a 10× LWD objective lens (375-039, Mitutoyo), a tube lens (AC254-100-A-ML, Thorlabs), and a high-resolution scientific CMOS camera (pco. panda 4.2, PCO). The output of the microscope was displayed on a computer screen for visual verification.

2.9. Histological Analysis. All tracheal samples, including both control and treated groups, were fixed in 4% paraformaldehyde prepared in 1× PBS (pH 7.4) at 4 °C overnight. Following fixation, the tissues were dehydrated through a graded series of isopropyl alcohol (IPA) solutions (80, 90, 95, and 100%) and CitriSolv solution (cat. no. 1061, Decon) before paraffin embedding. The paraffin-embedded tissues were sectioned into thin slices of 5−8 μm thickness. These sections were subsequently deparaffinized with CitriSolv and rehydrated through a descending IPA gradient (100, 95, 90, 80, 70, and 50%). Finally, the tissue sections were stained with hematoxylin and eosin (H&E) and imaged for microscopic evaluation of the epithelial and subepithelial layers.

2.10. Tissue Viability Assay. Tissue viability before and after osmo-mechanical treatment was assessed using the LIVE/DEAD viability/cytotoxicity kit (cat. no. L3224, Invitrogen) in accordance with the manufacturer protocol. Briefly, the trachea samples were incubated in 1 mL of 1× PBS containing 10 μM calcein AM and 20 μM ethidium homodimer-1 (EthD-1) for 15 min. After staining, the samples were washed again with 1× PBS. Fluorescence imaging was performed using an Olympus BX51 microscope with excitation/emission wavelengths of 494/517 nm for live cells and 528/617 nm for dead cells. The acquired images were analyzed with ImageJ software (National Institutes of Health, Bethesda, MD), and cell viability was calculated as the percentage of live cells relative to the total cell count using the following equation:

$$\text{cell viability (\%)} = \frac{\text{No. of live cells}}{\text{No. of live cells} + \text{No. of dead cells}} \times 100$$

2.11. Statistical Analysis. Statistical analysis was performed using GraphPad Prism (GraphPad Software, Inc., La Jolla, CA, USA). All data were presented as the mean ± standard deviation ($n \geq 3$). Statistical differences were assessed by one-way ANOVA with Tukey's multiple comparison posthoc test. Differences were considered to be statistically significant at $p < 0.05$.

3. RESULTS

3.1. Characterization of the Mechanical Vibrational Force. For the experiment, we utilized isolated rat tracheal tissue exposed to HTS in a Petri dish (Figure 2A). To induce vibration, we employed a custom-designed shaker controlled by a computer-generated sinusoidal waveform whose output was continuously monitored by an accelerometer for accuracy (Figure 2B). We used the accelerometer to measure the acceleration of the vibrational force overtime both at the actuator and the tissue. The acceleration of the sinusoidal wave demonstrated a minor 9% reduction in the vibrational force as it propagates from the actuator to the tissue through a sample stage (Figure 2C). The amplitude of the wave indicates the maximum acceleration, which was recorded to be approximately 0.69 gravity force (F_g) at the actuator to 0.62 F_g at the tissue.

Therefore, the mechanical oscillation of 70 Hz with a maximum acceleration of around 0.6 F_g could transiently permeabilize the airway epithelial TJ (Figure 2D). Notably, this vibration frequency used in the experiment is approximately in a clinically accepted range of 20−65 Hz used in mechano-acoustic device for airway clearance techniques.[26−28] Overall, we will explore the combined effect of osmosis and vibrational force in enabling paracellular permeability for more effective drug delivery to the airway epithelium.

3.2. Synergistic Effect of HTS and Oscillation on ZO-1. To visually and quantitatively assess the impact of combined osmo-mechanical treatment on TJ integrity in airway tissue, zonula occludens-1 (ZO-1) was stained using immunofluorescence. The resulting fluorescent images were analyzed to compare ZO-1 distribution across three conditions: unexposed tissue, tissue exposed to hypertonic saline (1.8% NaCl) alone, and tissue treated with hypertonic saline combined with 70 Hz vibration for 30 min (Figure 3A). The airway tissue (control)

https://doi.org/10.1021/acsbiomaterials.5c01104
ACS Biomater. Sci. Eng. XXXX, XXX, XXX−XXX

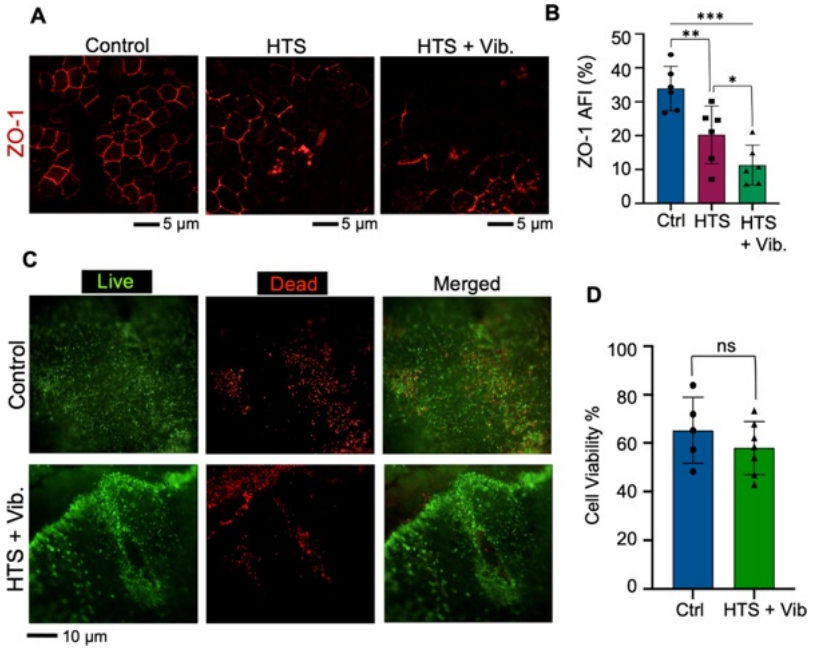

Figure 3. Effect of hypertonic solution and vibration on ZO-1 localization in the rat trachea. (A) Representative fluorescent images of rat tracheal whole-mount stain for tight junction protein zonula occludens-1 (ZO-1) following exposure to hypertonic saline (HTS) 1.8% NaCl only and combined with 70 Hz vibration for 30 min. (B) Quantification of the ZO-1 distribution was based on the area fraction index (AFI) derived from fluorescence images, where the AFI is calculated as the percentage of pixels in the fluorescence image with specified intensity values relative to the total number of pixels. (C) Representative fluorescence images from the live and dead assay demonstrating tissue viability, where green indicates live cells and red indicates dead cells. Images were captured using a conventional fluorescence microscope to evaluate the effect of treatment on the tissue viability. (D) Quantification of cell viability, expressed as the percentage of live cells relative to the total cell count, showed no significant difference between the control and treated group. Vib.: vibration. $*p < 0.05$. $**p < 0.01$. $***p < 0.001$. ns: not significant.

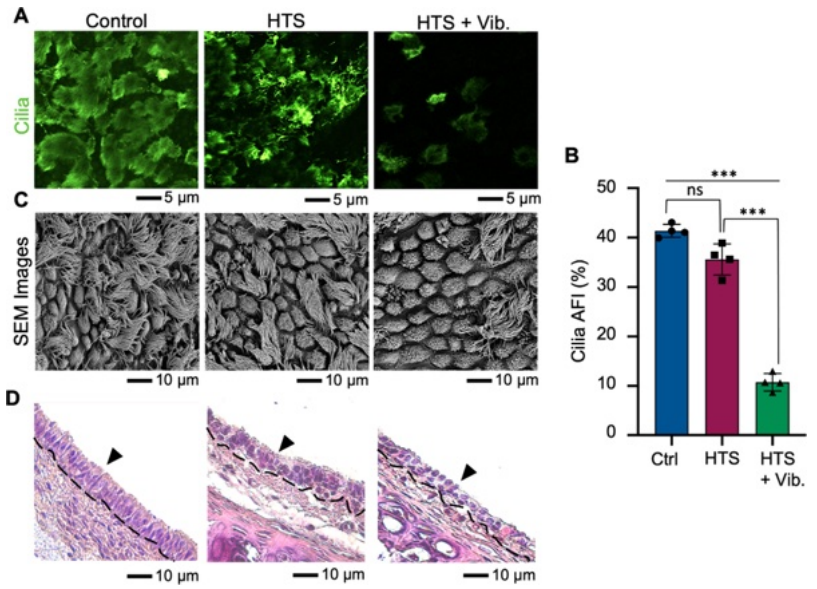

Figure 4. Impact of hypertonic saline and vibration on the ciliary structure in the rat trachea. (A) Fluorescent images of rat tracheal whole mounts stained for acetylated α-tubulin to visualize cilia without any treatment and following exposure to hypertonic saline (HTS) 1.8% NaCl only or in combination with 70 Hz vibration for 30 min. (B) Quantification of ciliary density based on the area fraction index (AFI), where the AFI is the ratio of pixels with intensity values above a specified threshold to the total number of pixels in the fluorescence image. (C) Scanning electron microscopy (SEM) images depicting the luminal surface of rat tracheae exposed to HTS 1.8% NaCl only or in combination with 70 Hz vibration for 30 min. (D) Representative H&E-stained sections demonstrating the effect of osmo-mechanical treatment on cilia and tracheal epithelium in control, HTS-treated, and HTS + vibration-treated groups. Vib.: vibration. $***p < 0.001$. ns: not significant.

with no treatment shows intact distribution of ZO-1 along the epithelial cells, indicating a preserved TJ structure. However, in the tissue with HTS treatment only, the distribution and localization of ZO-1 protein showed empty spaces surrounded by disrupted pattern of ZO-1 distribution. The group with HTS in combination with 70 Hz vibration further showed decreased in staining intensity and potential redistribution of

https://doi.org/10.1021/acsbiomaterials.5c01104
ACS Biomater. Sci. Eng. XXXX, XXX, XXX−XXX

the protein. This suggests that the combined treatment has had a more significant impact on compromising TJ integrity.

To quantitatively assess the visual changes in ZO-1 localization, we calculated the area fraction index (AFI) of ZO-1 signals in the fluorescent images (Figure 3B). AFI is the ratio of the total number of pixels above a specified threshold (min value: 39 intensity and max value: 255 intensity) to the total number of pixels in the image.[29] This metric provides a numerical measure of the relative abundance of ZO-1 within the tissue. The AFI of ZO-1 in native untreated tissue samples was approximately 32%, indicating the substantial presence of the intact ZO-1 protein. Exposure to HTS alone significantly decreased AFI to around 20%, likely due to ZO-1 disruption and loss of the fluorescence signal. Notably, the combination of HTS and vibration further reduced the AFI to nearly 11%. This suggests that vibration exacerbated the disruptive effects of HTS on TJ, potentially leading to both the disruption of ZO-1 localization and a decrease in its abundance.

To assess the impact of osmo-mechanical treatment on overall epithelial integrity and tissue viability, the LIVE/DEAD cell viability assay was performed. The fluorescence imaging of tracheal sections showed that cells remained largely unaffected by the treatments (Figure 3C and Figure S1). Quantitative analysis of live cells (green) and dead cells (red) revealed similar proportions of viable cells in both control and treated tissues (Figure 3D), indicating that exposure to hypertonic saline combined with a 70 Hz vibration did not significantly compromise overall cell viability.

3.3. Combination Effects of HTS and Vibration on the Cilium Structure. To study the effect of the treatment on the cilium structure, we performed immunofluorescent staining of the rat trachea for acetylated α-tubulin, a protein marker for cilia. The confocal microscopy images were acquired and analyzed to compare for the distribution of cilia in tissues that were exposed to HTS alone and in combination with 70 Hz vibration for 30 min (Figure 4A). In the untreated control samples, the cilia were observed to be evenly distributed along the apical surface of epithelial cells. However, both treatment groups exhibited notable alterations in the ciliary morphology, orientation, and density. While HTS treatment alone did not significantly affect ciliary density, it did induce ciliary disorganization and detachment. In contrast, the combination of HTS and vibration resulted in a marked decrease in ciliary density, indicating that the combined treatment disrupted the ciliary structure.

To quantitatively assess changes in ciliary density, we calculated the AFI of ciliary staining in the fluorescent images (Figure 4B). The AFI provides a numerical measure of the relative abundance of cilia within the tissue. In native tissue, the AFI of cilia was approximately 41%, indicating a relatively high density and well-organized structure. This value was reduced to 35% in samples treated with HTS alone, likely due to ciliary disorganization. However, when vibration was applied in combination with HTS, the ciliary AFI dropped to approximately 10%. This reduction reflects a substantial decrease in the ciliary density and changes in ciliary morphology.

To visually confirm the changes observed in immunofluorescence, we employed scanning electron microscopy (SEM) to examine the luminal surface of the rat trachea (Figure 4C). This will allow for a detailed examination of the ciliary architecture. SEM images revealed a trend similar to that observed in the immunofluorescent images, revealing variations in ciliary density. The native rat trachea exhibits a dense ciliary structure. While the treated group with HTS and vibration revealed morphological abnormalities such as shortened or damaged cilia along with ciliary detachment. These changes would suggest the effect of treatment on mucociliary function.

The H&E (hematoxylin and eosin) histology staining (Figure 4D) confirmed the structural alterations observed in both immunofluorescence and SEM imaging. The native trachea epithelium displayed an intact, well-organized ciliary layer along the apical surface with closely packed epithelial cells maintaining normal morphology. In contrast, tissues treated with HTS alone exhibited partial ciliary detachment and disorganization along with subtle widening of the intercellular spaces. These effects were much more pronounced in the HTS + vibration group, where cilia were frequently shortened, fragmented, or completely absent. Furthermore, epithelial cells in the osmo-mechanical treatment group appeared shrunken and irregularly spaced, indicating substantial structural disruption of the epithelium and highlighting the pronounced impact of the treatment on tissue architecture.

3.4. Quantification of the Effects of Tissue Permeability on Tissue Bioimpedance. We investigated whether the permeability of the tissues altered via the treatments can be evaluated by measuring the electrical properties, in particular, bioelectrical impedance (bioimpedance), of the airway epithelium. Based on the mechanism of current flow through tissue, that at low frequencies, current primarily flows through the extracellular fluid, bypassing cell membranes, while at high frequencies, capacitive pathways dominate, enabling current to pass through cell membranes.[30] Therefore, we hypothesized that at when high-frequency current flows is supplied, tissue with intact intracellular junctions would impede the flow of electrical current, leading to higher resistance, while disrupted tissue with compromised intracellular junctions would allow for easier current flow, resulting in decreased resistance[31] (Figure 5A).

To accomplish this, we constructed a bioelectrical measurement platform that employs a four-point electrode configuration[31] (Figure 5B). An alternating current (AC) of varying frequencies (250 Hz to 135 kHz) was applied, and the resulting potential distribution was measured on native tissue and treated tissue samples[31] (Figure 5C). Bioimpedance of the samples was calculated across the frequency range, while the bioimpedance values measured from different tissue samples were analyzed at 120 kHz.

The results demonstrated a significant decrease in a bioimpedance of about $6.0 \times 10^2\ \Omega$ in the HTS alone group compared to the $9.0 \times 10^2\ \Omega$ in the control group (Figure 5D). This suggests that the HTS alone disrupts the tissue's electrical properties by permeabilizing the intracellular junctions. Furthermore, the HTS combined with vibration groups exhibited an even lower bioimpedance of nearly $4.5 \times 10^2\ \Omega$ compared to $6.0 \times 10^2\ \Omega$ of the HTS alone group, indicating that the addition of vibration further enhances alteration in the electrical properties. This suggests that the combined effect of HTS and vibration is more potent in altering the tissue permeability.

3.5. Assessing the Treatment-Induced Change in the Airway Epithelial Permeability. A dextran penetration assay was conducted to quantify the increase in permeability caused by TJ disruption.[32] Fluorescein isothiocyanate−dextran (FITC-Dextran), a versatile fluorescent tracer, was applied to

https://doi.org/10.1021/acsbiomaterials.5c01104
ACS Biomater. Sci. Eng. XXXX, XXX, XXX−XXX

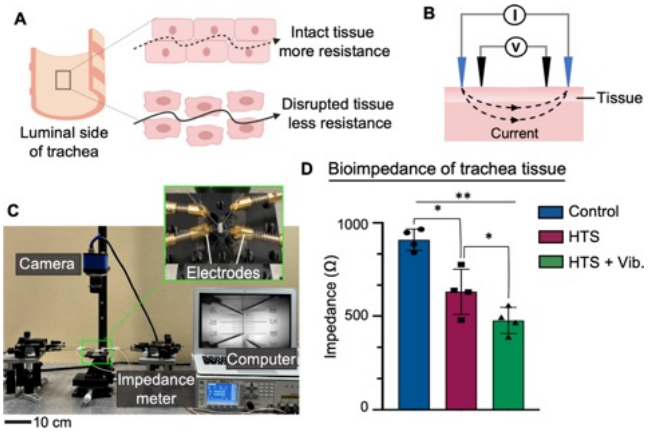

Figure 5. Bioimpedance measurement for assessing tight junction disruption in the rat trachea. (A) Schematic representation of electrical current flow through intact and disrupted airway tissue. (B) Cross-sectional view of the rat trachea with a four-probe bioimpedance measurement system. (C) Experimental setup for measuring bioimpedance of airway tissue, including electrodes, an impedance meter, and a computer. (D) Bar graph illustrating changes in bioimpedance of trachea tissue at 120 kHz alternating current frequency for control, HTS only, and HTS combined with the 70 Hz vibration experimental groups. Vib.: vibration. *p < 0.05. **p < 0.01.

the apical surface of the airway epithelium. Its penetration depth was measured using z-stack confocal imaging over 15 min (Figure 6A). The localized concentration gradient drove dextran diffusion through the tissue, facilitated by open TJs.[33] The distance traveled by dextran molecules was used to estimate the epithelial barrier permeability and the effectiveness of TJ disruption treatments. XZ plane views of dextran

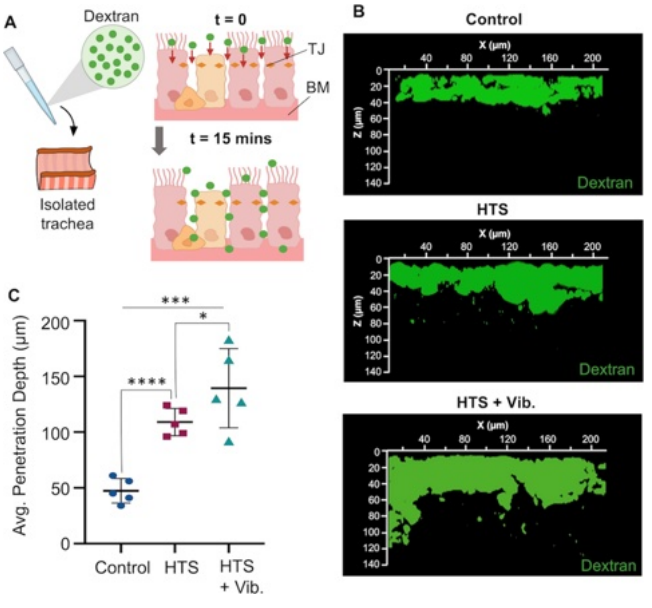

Figure 6. Dextran incorporation in airway tissue. (A) Schematics of the mechanism of dextran penetration through the open tight junctions in airway. (B) XZ plane view of the dextran penetration in hypertonic solution (HTS) and HTS with vibration, green fluorescence is that of dextran. (C) Graphical representation of the average (average) penetration depth by dextran in different experimental groups. Vib.: vibration *p < 0.05. ***p < 0.001. ****p < 0.0001.

penetration in the control, HTS, and HTS with vibration groups were obtained with green fluorescence indicating the presence of dextran (Figure 6B). The results demonstrate a significant enhancement of dextran penetration in both treated groups compared with the control. This suggests that the treatments effectively disrupt TJs, creating a more permeable pathway for drug molecules to reach the underlying tissues.

To obtain a comprehensive understanding of dextran penetration, the average penetration depth was calculated from multiple experiments and graphically represented (Figure 6C). The average distance covered by the dextran in HTS with vibration groups was approximately 139.4 ± 35.5 μm, which was much higher than the depth traveled by dextran in control (47.4 ± 11.0 μm). Expectedly, dextran penetration was slightly lower in the HTS-only group (109.0 ± 12.2 μm) than in the HTS with vibration groups. These data further confirm the increased permeability induced by the combined HTS and vibration treatment to significantly enhance the drug delivery.

4. DISCUSSION

In this study, we investigated the combined effects of HTS and vibration as a potential strategy to modulate the airway epithelial permeability that can promote drug or gene delivery to the cells in the sub epithelial regions. A significant challenge is the location of the basal cells, which are anchored to the basal membrane beneath the pseudostratified epithelial cells of the airway. The epithelial cells form a semipermeable barrier due to the presence of TJs between them, creating a formidable obstacle for drug delivery.[34,35] Disrupting the integrity of TJs using the combined application of HTS and vibration can increase permeability, potentially facilitating drug delivery to underlying tissues (Figures 1 and 2). The viability assay indicates that the treatment preserves overall tissue viability with similar proportions of live cells in both control and treated tissues (Figure 3C,D). The maintained cellular health suggests that the treated tissue could potentially be maintained in culture over extended periods, enabling future studies on epithelial recovery. We used confocal microscopy and electron beam microscopy to visualize and quantify the structural changes in the airway epithelium caused by this osmo-mechanical treatment. Furthermore, we characterized the electrical properties of the tissue using bioimpedance measurements and the permeability characteristics using dextran incorporation to further understand the impact of this treatment on drug delivery.

The confocal images revealed a significant disruption of TJs in airway epithelial tissue following treatment with the HTS and vibration (Figure 3), indicated by structural changes and a decreased abundance of ZO-1. To further explore the effect of the osmo-mechanical treatment on the epithelium, we quantified changes in the cilium structure (Figure 4). High-frequency vibration, in particular, can induce mechanical stress on the cilia, leading to detachment from the apical membrane.[36] This stress may result from the rapid oscillation of the vibrating surface, which can disrupt the adhesive forces between the cilia and the underlying cell membrane. Additionally, high-frequency vibration may generate shear forces that can physically tear the cilia away.[36] While HTS (sodium chloride, NaCl) is generally considered less damaging to the airway epithelium compared to other substances, it can still cause some degree of irritation and inflammation.[37] Prolonged exposure to high concentrations of NaCl can lead to osmotic stress, which can disrupt cellular homeostasis and

https://doi.org/10.1021/acsbiomaterials.5c01104
ACS Biomater. Sci. Eng. XXXX, XXX, XXX−XXX

potentially contribute to cilium detachment.[37,38] The H&E histology (Figure 4D) confirmed that these conditions led to notable changes in epithelial morphology with partial to extensive ciliary loss and detachment. Additionally, in control tissues, epithelial cells were tightly arranged and exhibited normal morphology, whereas in tissues subjected to the osmo-mechanical treatment, the cells appeared shrunken, and the intercellular spaces were noticeably widened, indicating the effect of osmosis on tissue architecture.

The confocal and SEM images provided compelling evidence of ciliary disruption in airway epithelial tissue following the treatment (Figure 4C). While these changes may temporarily impair mucociliary clearance, it is important to note that cilia are highly regenerative structures and can readily recover following tissue damage.[39−42] The ability of cilia to regenerate is crucial for maintaining normal airway function and preventing the accumulation of mucus and debris. Therefore, the temporary disruption of the cilia, coupled with the potential for rapid regeneration, suggests that this treatment creates a transient pathway for drug delivery.

We further showed that disruption of the TJs between the epithelial cells caused by the physical tissue damage can be quantified by measuring the electrical properties of the local airway tissue[30,31] (Figure 5). A significant decrease in bioimpedance was observed in both the HTS-only and HTS with vibration groups compared with the control group, indicating a disruption of tissue electrical properties. This reduction in bioimpedance is likely attributed to the increased tissue permeability, which allows for easier current flow. The relationship between bioimpedance and tissue permeability can be understood in terms of the electrical properties of the tissue. In tissues with intact intracellular junctions, the electrical current encounters greater resistance due to the presence of barriers that impede its flow. These barriers include cell membranes, TJ, and other cellular structures.[31,43] When tissue permeability increases, these barriers are disrupted or compromised, allowing for easier current flow. This reduced resistance leads to a decrease in bioimpedance.[31] The observed changes in bioimpedance are consistent with the findings from the confocal and SEM images, which demonstrated disruptions in the TJ structure. These results collectively highlight the ability of bioimpedance measurements to serve as a non-invasive and sensitive indicator of tissue damage and alterations in permeability.

To further check the permeability of the pathway created by this osmo-mechanical treatment, we performed a dextran penetration assay (Figure 6). The dextran was chosen as a tracer molecule as it is a highly hydrophilic molecule that can readily interact with water molecules, forming a hydrated layer around its structure.[44] This hydration layer facilitates the diffusion of dextran across biological barriers, such as epithelial tissues, allowing a precise measurement of paracellular diffusion. We incorporated FITC-dextran (molecular weight: 4 kDa) into the tissues for this assay. This molecular weight falls within a range that is optimal for penetrating epithelial tissues without being excessively large or small.[33] Larger dextran molecules might face greater resistance in diffusing through tissue barriers, while smaller molecules could be more readily cleared before reaching the target tissues. Therefore, FITC-dextran represents a well-balanced choice for permeability assays, providing a reliable and informative measure of tissue barrier function.[32]

Based on the histological cross-section image analysis from the previous literature, we calculated rat tracheal tissue width to be approximately 150−250 μm. The epithelial cell layer thickness within this measurement ranges from 30 to 50 μm.[36,45,46] The basal cells are located at the base of the basal membrane. Dextran penetration depth serves as a valuable indicator of epithelial layer permeability by calculating the distance traveled.[32,33,47] In the treated groups, dextran penetration extended well beyond the epithelial layer, with some regions demonstrating higher penetration, potentially due to nonuniform injury and slight visualization inconsistencies caused by the trachea's curvature. These observations highlight the potential of the treatment to enhance epithelial permeability and suggest future research exploring the delivery of larger molecules. Additionally, the distribution of dextran within the tissue can be analyzed to provide insights into the heterogeneity of permeability changes. For instance, a more widespread distribution of dextran indicates a uniform disruption of the TJ across the epithelial surface. This could be particularly important for applications where a consistent permeability is desired.

Building on the findings of this study, our future work will focus on evaluating the restoration of tight junctions and epithelial integrity by using a controlled bioreactor system. While this study demonstrates a method to enhance epithelial permeability using hypertonic saline and vibration, assessing the reversibility remains a key goal for future investigations for advancing the translational potential of this approach.

5. CONCLUSIONS

In conclusion, our study investigated the effects of HTS and vibration on airway epithelial TJ and their subsequent impact on drug delivery and mucociliary function. We demonstrated that the combined treatment significantly disrupted the TJ, leading to increased paracellular permeability and enhanced drug delivery. The confocal and SEM images showed a redistribution of proteins and cilium structure. Bioimpedance measurements confirmed these findings, as indicated by the decrease in the electrical resistance (i.e., bioimpedance) of the tissue following treatment. Future studies would explore strategies to optimize the treatment regimen that can transiently modulate the TJ integrity with minimal tissue injury. Overall, our findings provide valuable insights into the potential of HTS and vibration as tools for modulating airway epithelial permeability and subsequent gene or drug delivery to subepithelial regions of the airway tissue.

■ ASSOCIATED CONTENT

Supporting Information

The Supporting Information is available free of charge at https://pubs.acs.org/doi/10.1021/acsbiomaterials.5c01104.

DAPI and ZO-1 staining of rat trachea following hypertonic solution and vibration treatment (Figure S1) (PDF)

■ AUTHOR INFORMATION

Corresponding Author

Jinho Kim − *Department of Biomedical Engineering, Stevens Institute of Technology, Hoboken, New Jersey 07030, United States;* orcid.org/0000-0002-4692-4407; Email: jkim6@stevens.edu

https://doi.org/10.1021/acsbiomaterials.5c01104
ACS Biomater. Sci. Eng. XXXX, XXX, XXX−XXX

Authors

Aneri Patel − *Department of Biomedical Engineering, Stevens Institute of Technology, Hoboken, New Jersey 07030, United States*

Jiawen Chen − *Department of Biomedical Engineering, Stevens Institute of Technology, Hoboken, New Jersey 07030, United States*

Mohammad Mir − *Department of Biomedical Engineering, Stevens Institute of Technology, Hoboken, New Jersey 07030, United States;* orcid.org/0000-0001-7828-3061

Maria R. Hudock − *Department of Biomedical Engineering, Columbia University, New York, New York 10027, United States;* orcid.org/0000-0001-5854-0761

Meghan R. Pinezich − *Department of Biomedical Engineering, Columbia University, New York, New York 10027, United States*

Ya-Wen Chen − *Department of Otolaryngology, Department of Stem Cell Biology and Regenerative Medicine, Black Family Stem Cell Institute, Institute for Airway Sciences, and Center for Epithelial and Airway Biology and Regeneration, Icahn School of Medicine at Mount Sinai, New York, New York 10029-5674, United States*

Matthew Bacchetta − *Department of Cardiac Surgery, Vanderbilt University, Nashville, Tennessee 37232-2102, United States*

Gordana Vunjak-Novakovic − *Department of Biomedical Engineering, Columbia University, New York, New York 10027, United States; Department of Medicine, Columbia University, New York, New York 10032, United States*

Complete contact information is available at: https://pubs.acs.org/10.1021/acsbiomaterials.5c01104

Author Contributions

The manuscript was written through contributions of all authors. All authors approved the final version of the manuscript.

Funding

The work was supported by the National Science Foundation (CAREER award no. 2143620 to J.K.) and the Cystic Fibrosis Foundation (Pioneer grant no. VUNJAK23XX0 to G.V.-N., J.K., and M.B.).

Notes

The authors declare no competing financial interest.

■ ACKNOWLEDGMENTS

The authors would like to thank Drs. Tsengming (Alex) Chou and Matthew Libera at Stevens Laboratory for Multiscale Imaging (LMSI) for their assistance with SEM imaging of the tissue samples.

■ ABBREVIATIONS

TJ,tight junction; HTS,hypertonic saline; PBS,phosphate buffer saline; SEM,scanning electron microscopy; ZO-1,zonula occludens-1; AFI,area fraction index; AC,alternating current; FITC-Dextran,fluorescein isothiocyanate-dextran

■ REFERENCES

(1) Scheuch, G.; Kohlhaeufl, M. J.; Brand, P.; Siekmeier, R. Clinical perspectives on pulmonary systemic and macromolecular delivery. *Adv. Drug Deliv Rev.* **2006**, *58* (9−10), 996−1008.

(2) Hertel, S. P.; Winter, G.; Friess, W. Protein stability in pulmonary drug delivery via nebulization. *Adv. Drug Deliv Rev.* **2015**, *93*, 79−94.

(3) Ruiz, M. E; Scioli-Montoto, S. Routes of drug administration. In *ADME Processes in Pharmaceutical Sciences: Dosage, Design, and Pharmacotherapy*; Springer, 2024; pp 129−172,

(4) Neary, M. T.; Mulder, L. M.; Kowalski, P. S.; MacLoughlin, R.; Crean, A. M.; Ryan, K. B. Nebulised delivery of RNA formulations to the lungs: From aerosol to cytosol. *J. Controlled Release* **2024**, *366*, 812−833.

(5) Jang, M.; Yeom, K.; Han, J.; Fagan, E.; Park, J. H. Inhalable mRNA Nanoparticle with Enhanced Nebulization Stability and Pulmonary Microenvironment Infiltration. *ACS Nano* **2024**, *18* (35), 24204−24218.

(6) Suberi, A.; Grun, M. K.; Mao, T.; Israelow, B.; Reschke, M.; Grundler, J.; Akhtar, L.; Lee, T.; Shin, K.; Piotrowski-Daspit, A. S.; Homer, R. J.; Iwasaki, A.; Suh, H. W.; Saltzman, W. M. Polymer nanoparticles deliver mRNA to the lung for mucosal vaccination. *Sci. Transl. Med.* **2023**, *15* (709), No. eabq0603.

(7) Verma, N. K.; Crosbie-Staunton, K.; Satti, A.; Gallagher, S.; Ryan, K. B.; Doody, T.; McAtamney, C.; MacLoughlin, R.; Galvin, P.; Burke, C. S.; Volkov, Y.; Gun'ko, Y. K. Magnetic core-shell nanoparticles for drug delivery by nebulization. *J. Nanobiotechnol.* **2013**, *11*, 1−12.

(8) Labiris, N. R.; Dolovich, M. B. Pulmonary drug delivery. Part I: physiological factors affecting therapeutic effectiveness of aerosolized medications. *Br. J. Clin. Pharmacol.* **2003**, *56* (6), 588−599.

(9) Uchenna Agu, R.; Ikechukwu Ugwoke, M.; Armand, M.; Kinget, R.; Verbeke, N. The lung as a route for systemic delivery of therapeutic proteins and peptides. *Respir. Res.* **2001**, *2*, 1−12.

(10) Bajracharya, R.; Song, J. G.; Back, S. Y.; Han, H. K. Recent advancements in non-invasive formulations for protein drug delivery. *Comput. Struct. Biotechnol. J.* **2019**, *17*, 1290−1308.

(11) Patton, J. S. Mechanisms of macromolecule absorption by the lungs. *Adv. Drug Delivery Rev.* **1996**, *19* (1), 3−36.

(12) Hussain, A.; Arnold, J. J.; Khan, M. A.; Ahsan, F. Absorption enhancers in pulmonary protein delivery. *J. Controlled Release* **2004**, *94* (1), 15−24.

(13) Gizurarson, S. The effect of cilia and the mucociliary clearance on successful drug delivery. *Biol. Pharm. Bull.* **2015**, *38* (4), 497−506.

(14) Houtmeyers, E.; Gosselink, R.; Gayan-Ramirez, G.; Decramer, M. Regulation of mucociliary clearance in health and disease. *Eur. Respir. J.* **1999**, *13* (5), 1177−1188.

(15) Marttin, E.; Schipper, N. G. M.; Verhoef, J. C.; Merkus, F. W. H. M. Nasal mucociliary clearance as a factor in nasal drug delivery. *Adv. Drug Delivery Rev.* **1998**, *29* (1−2), 13−38.

(16) Kojima, T.; Go, M.; Takano, K. i.; Kurose, M.; Ohkuni, T.; Koizumi, J. i.; Kamekura, R.; Ogasawara, N.; Masaki, T.; Fuchimoto, J.; Obata, K.; Hirakawa, S.; Nomura, K.; Keira, T.; Miyata, R.; Fujii, N.; Tsutsumi, H.; Himi, T.; Sawada, N. Regulation of Tight Junctions in Upper Airway Epithelium. *BioMed Res. Int.* **2013**, *2013*, No. 947072.

(17) Mohammed, M. A.; Syeda, J. T. M.; Wasan, K. M.; Wasan, E. K. An overview of chitosan nanoparticles and its application in non-parenteral drug delivery. *Pharmaceutics* **2017**, *9* (4), 53.

(18) Wang, G.; Zabner, J.; Deering, C.; Launspach, J.; Shao, J.; Bodner, M.; Jolly, D. J.; Davidson, B. L.; McCray, P. B., Jr. Increasing epithelial junction permeability enhances gene transfer to airway epithelia in vivo. *Am. J. Respir. Cell Mol. Biol.* **2000**, *22* (2), 129−138.

(19) Miwa, M.; Matsunaga, M.; Nakajima, N.; Yamaguchi, S.; Watanabe, K. Hypertonic saline alters electrical barrier of the airway epithelium. *Otolaryngol., Head Neck Surg.* **2007**, *136* (1), 62−66.

(20) Nilsson, H.; Dragomir, A.; Ahlander, A.; Johannesson, M.; Roomans, G. M. Effects of hyperosmotic stress on cultured airway epithelial cells. *Cell Tissue Res.* **2007**, *330* (2), 257−269.

(21) Brunner, J.; Ragupathy, S.; Borchard, G. Target specific tight junction modulators. *Adv. Drug Delivery Rev.* **2021**, *171*, 266−288.

(22) Deli, M. A. Potential use of tight junction modulators to reversibly open membranous barriers and improve drug delivery. *Biochim. Biophys. Acta Biomembr.* **2009**, *1788* (4), 892−910.
(23) McIlwaine, M. Physiotherapy and airway clearance techniques and devices. *Paediatr. Respir. Rev.* **2006**, *7*, S220−S222.
(24) Högman, M.; Mörk, A. C.; Roomans, G. M. Hypertonic saline increases tight junction permeability in airway epithelium. *Eur. Respir. J.* **2002**, *20* (6), 1444−1448.
(25) Relova, A. J.; Roomans, G. M. Effect of luminal osmolarity on ion content of connective tissue in rat trachea after epithelial damage. *Eur. Respir. J.* **2001**, *18* (5), 810−816.
(26) Song, M.; Kwon, S. Enhanced Cellular Permeation Efficiency Through Mechanical Vibration-induced Actin Cytoskeleton Changes in Human Nasal Epithelial Cells. *Biotechnol Bioproc E* **2021**, *26*, 1034−1042.
(27) Uzundurukan, A.; Poncet, S.; Boffito, D. C.; Micheau, P. Acoustic airway clearance devices: A systematic review of experimental and numerical studies. *Biomed. Eng. Adv.* **2024**, *8*, No. 100134.
(28) Schieppati, D.; Germon, R.; Galli, F.; Rigamonti, M. G.; Stucchi, M.; Boffito, D. C. Influence of frequency and amplitude on the mucus viscoelasticity of the novel mechano-acoustic Frequencer. *Respir Med.* **2019**, *153*, 52−59.
(29) Canfield, S. G.; Stebbins, M. J.; Morales, B. S.; Asai, S. W.; Vatine, G. D.; Svendsen, C. N.; Palecek, S. P.; Shusta, E. V. An isogenic blood-brain barrier model comprising brain endothelial cells, astrocytes, and neurons derived from human induced pluripotent stem cells. *J. Neurochem* **2017**, *140* (6), 874−888.
(30) Amini, M.; Hisdal, J.; Kalvoy, H. Applications of Bioimpedance Measurement Techniques in Tissue Engineering. *J. Electr Bioimpedance* **2018**, *9* (1), 142−158.
(31) Kim, J.; Chen, J.; Mir, S.; Hudock, M.; Pinezich, M.; Chen, P.; Patel, A.; Bacchetta, M.; Vunjak-Novakovic, G. Opto-Electrical Quantification of Airway Epithelial Injury. *Am. J. Respir. Crit. Care Med.* **2023**, 207.
(32) Chen, H.; Wu, S.; Lu, R.; Zhang, Y. G.; Zheng, Y.; Sun, J. Pulmonary permeability assessed by fluorescent-labeled dextran instilled intranasally into mice with LPS-induced acute lung injury. *PLoS One* **2014**, *9* (7), No. e101925.
(33) Matsukawa, Y.; Lee, V. H.; Crandall, E. D.; Kim, K. J. Size-dependent dextran transport across rat alveolar epithelial cell monolayers. *J. Pharm. Sci.* **1997**, *86* (3), 305−309.
(34) Rock, J. R.; Onaitis, M. W.; Rawlins, E. L.; Lu, Y.; Clark, C. P.; Xue, Y.; Randell, S. H.; Hogan, B. L. Basal cells as stem cells of the mouse trachea and human airway epithelium. *Proc. Natl. Acad. Sci. U. S. A.* **2009**, *106* (31), 12771−12775.
(35) Donnelley, M.; Parsons, D. W. Gene Therapy for Cystic Fibrosis Lung Disease: Overcoming the Barriers to Translation to the Clinic. *Front Pharmacol* **2018**, *9*, No. 1381.
(36) Mir, M.; Chen, J.; Pinezich, M. R.; O'Neill, J. D.; Huang, S. X. L.; Vunjak-Novakovic, G.; Kim, J. Imaging-guided bioreactor for de-epithelialization and long-term cultivation of ex vivo rat trachea. *Lab Chip* **2022**, *22* (5), 1018−1031.
(37) Reeves, E. P.; McCarthy, C.; McElvaney, O. J.; Vijayan, M. S.; White, M. M.; Dunlea, D. M.; Pohl, K.; Lacey, N.; McElvaney, N. G. Inhaled hypertonic saline for cystic fibrosis: Reviewing the potential evidence for modulation of neutrophil signalling and function. *World J. Crit Care Med.* **2015**, *4* (3), 179−191.
(38) Shapiro, L.; Dinarello, C. A. Hyperosmotic Stress as a Stimulant for Proinflammatory Cytokine Production. *Exp. Cell Res.* **1997**, *231* (2), 354−362.
(39) Tadokoro, T.; Wang, Y.; Barak, L. S.; Bai, Y.; Randell, S. H.; Hogan, B. L. IL-6/STAT3 promotes regeneration of airway ciliated cells from basal stem cells. *Proc. Natl. Acad. Sci. U. S. A.* **2014**, *111* (35), E3641−3649.
(40) Gamm, U. A.; Huang, B. K.; Mis, E. K.; Khokha, M. K.; Choma, M. A. Visualization and quantification of injury to the ciliated epithelium using quantitative flow imaging and speckle variance optical coherence tomography. *Sci. Rep.* **2017**, *7* (1), 1−7.
(41) Kim, J. K.; Vinarsky, V.; Wain, J.; Zhao, R.; Jung, K.; Choi, J.; Lam, A.; Pardo-Saganta, A.; Breton, S.; Rajagopal, J.; Yun, S. H. In Vivo Imaging of Tracheal Epithelial Cells in Mice during Airway Regeneration. *Am. J. Respir. Cell Mol. Biol.* **2012**, *47* (6), 864−868.
(42) Keenan, K. P.; Wilson, T. S.; McDowell, E. M. Regeneration of Hamster Tracheal Epithelium after Mechanical Injury. *Virchows Arch. B Cell Pathol.* **1983**, *43*, 213−240.
(43) Dean, D. A.; Ramanathan, T.; Machado, D.; Sundararajan, R. Electrical Impedance Spectroscopy Study of Biological Tissues. *J. Electrostat* **2008**, *66* (3−4), 165−177.
(44) Díaz-Montes, E. Dextran: Sources, Structures, and Properties. *Polysaccharides* **2021**, *2* (3), 554−565.
(45) Hahn, A.; Faulhaber, J.; Srisawang, L.; Stortz, A.; Salomon, J. J.; Mall, M. A.; Frings, S.; Möhrlen, F. Cellular distribution and function of ion channels involved in transport processes in rat tracheal epithelium. *Physiol. Rep.* **2017**, *5* (12), No. e13290.
(46) Greaney, A. M.; Ramachandra, A. B.; Yuan, Y.; Korneva, A.; Humphrey, J. D.; Niklason, L. E. Decellularization compromises mechanical and structural properties of the native trachea. *Biomater. Biosyst.* **2023**, *9*, No. 100074.
(47) Bartosova, M.; Ridinger, D.; Marinovic, I.; Heigwer, J.; Zhang, C.; Levai, E.; Westhoff, J. H.; Schaefer, F.; Terjung, S.; Hildenbrand, G.; Krunic, D.; Bestvater, F.; Hausmann, M.; Schmitt, C. P.; Zarogiannis, S. G. An Experimental Workflow for Studying Barrier Integrity, Permeability, and Tight Junction Composition and Localization in a Single Endothelial Cell Monolayer: Proof of Concept. *International Journal of Molecular Sciences* **2021**, *22* (15), 8178.

https://doi.org/10.1021/acsbiomaterials.5c01104
ACS Biomater. Sci. Eng. XXXX, XXX, XXX−XXX